HHS Public Access

Author manuscript

J Prosthet Dent. Author manuscript; available in PMC 2021 August 09.

Published in final edited form as:

J Prosthet Dent. 2021 August ; 126(2): 238–247. doi:10.1016/j.prosdent.2020.05.023.

Effect of crystalline phase assemblage on reliability of 3Y-TZP

Isabelle Denry, DDS, MS, PhD[a] [Professor], Maged Abdelaal, DDS, MS[b] [Clinical Assistant Professor], Deborah V. Dawson, PhD[c] [Professor], Julie A. Holloway, DDS, MS[d] [Professor and Head], J. Robert Kelly, DDS, PhD[e] [Professor]

[a]Iowa Institute for Oral Health Research, University of Iowa College of Dentistry and Department of Prosthodontics, Iowa City, IA, USA

[b]Division of Prosthodontics, Department of General Dentistry, East Carolina University School of Dental Medicine, Greenville, NC, USA

[c]Department of Biostatistics, University of Iowa College of Public Health, Iowa City, IA, USA

[d]Department of Prosthodontics, University of Iowa College of Dentistry, Iowa City, IA, USA

[e]Department of Reconstructive Sciences, University of Connecticut Health Center, Farmington, CT

Abstract

Statement of problem.—Strengthening mechanisms of zirconia ceramics stabilized with 3 mol.% yttria (3Y-TZP) are complex and dictated by the crystalline phase assemblage. Although their clinical performance for dental restorations has been excellent, there is evidence that framework fractures do occur and are under-reported. Meanwhile there is a lack of understanding of the relationship between phase assemblage and reliability of 3Y-TZP.

Purpose.—To elucidate the relationship between crystalline phase assemblage and reliability of 3Y-TZP, and calculate associated probabilities of survival.

Material and methods.—Discs of 3Y-TZP were prepared from cylindrical blanks and randomly assigned to 12 experimental groups (n=20 per group). Different crystalline phase assemblages were produced by either varying sintering temperature from 1350 to 1600°C and/or treating the surface by airborne-particle abrasion with 50 μm alumina particles at a pressure of 2 bars for 1 minute with or without subsequent heat treatment. Crystalline phases were analyzed by standard and grazing incidence x-ray diffraction (GIXRD). The relationship between phase assemblage and reliability was determined by measuring the biaxial flexural strength (BFS) according to ISO standard 6872 and using Weibull statistics to calculate Weibull modulus (m), probability of survival and maximum allowable stresses. XRD results were analyzed by ANOVA to detect statistically significant differences between groups. Adjustment for all pairwise group comparisons was made using the Tukey method (0.05 level of significance).

Corresponding Author: Prof. Isabelle Denry , The University of Iowa College of Dentistry, 801 Newton Road, Iowa City, IA 52242, Phone: 1 (319) 335-7369, Facsimile: 1 (319) 335-8895, Isabelle-Denry@uiowa.edu.

Declarations of interest: none

Results.—Standard incidence XRD confirmed the presence of a small amount of cubic phase after sintering at 1350°C. A cubic-derived non-transformable tetragonal *t'*-phase was observed at sintering temperatures of 1450°C and above, the amount of which increased linearly. GIXRD revealed that airborne-particle abraded groups sintered at 1350 and 1600°C had the highest variability in monoclinic phase fraction as a function of depth, associated with the lowest reliability. Groups as-sintered at 1350 and 1600°C had the lowest modulus (*m*=8.1 (0.5) and 7.0 (0.8), respectively) and probability of survival (*Ps*) for a maximum allowable stress of 700 MPa, while treated groups sintered at 1450 and 1550°C were associated with the highest modulus (from 15.0 (1.4) to 20.9 (1.4)) and *Ps* ($\geq$ 0.9999). Lower strength and reliability of groups sintered at 1600°C was in line with the presence of a significant amount of non-transformable *t'*-phase. The pattern of BFS results indicated that ferro-elastic domain switching was a dominant strengthening mechanism in 3Y-TZP.

Conclusions.—The present study first reports on the detrimental effect of the cubic-derived non-transformable *t'*-phase on the mechanical properties of 3Y-TZP. It is demonstrated that phase assemblage determines reliability and is directly linked to the probability of survival.

INTRODUCTION

Despite the recent introduction of translucent zirconia compositions with larger amounts of yttrium stabilizer,[1, 2] zirconia ceramics stabilized with 3 mol.% yttria (3Y-TZP) are still extensively used for dental restorations and have been extremely successful.[3, 4] This is largely due to their excellent mechanical properties supported by the unique stress-induced transformation toughening, made possible by the stabilization of the tetragonal phase.[5-7] 3Y-TZP ceramics are therefore very attractive for posterior restorations where strength is critical.[8, 9] However, depending on the manufacturer, sintering conditions for 3Y-TZP vary widely, with temperatures ranging from 1350 to 1600°C. Meanwhile, it is well established that sintering conditions such as temperature and duration strongly affect grain size, crystallographic phase assemblage and stabilizer distribution in zirconia ceramics.[10, 11] In addition, the transformability of 3Y-TZP is directly linked to grain size.[10-13] For example, Suresh and Mayo[13] determined that for 3Y-TZP pellets, the critical grain size below which the tetragonal phase remains stable is 155 nm, whereas larger grain sizes have a greater propensity to transform to the monoclinic phase,[11] with grains larger than 5-6 μm spontaneously switching to the monoclinic phase upon cooling. Furthermore, the amount of stable cubic phase increases with sintering temperature and its presence is associated with a decrease in strength due to its inability to transform.[10] Therefore, starting from chemically similar zirconia powders stabilized with 3 mole percent yttria (3Y-TZP), variations in sintering recommendations are expected to lead to notable differences in microstructural characteristics and crystalline phase assemblage, directly affecting transformability and thereby mechanical properties and reliability of definitive restorations in various clinical scenarios.[14] In order to improve mechanical retention, indirect dental restorations such as single crowns or fixed partial prostheses are usually airborne-particle abraded (AA) prior to cementation.[15, 16] This type of surface treatment is well documented in the literature and has been shown to trigger the expected stress-induced *t-m* transformation and lead to a significant increase in mean biaxial flexural strength for both fine and coarse-grained 3Y-TZP.[17, 18] It was later shown that AA was also associated with higher survival rates for 3Y-

TZP under cyclic loading.[19] The beneficial effect of AA on the resistance of 3Y-TZP to low temperature degradation was further demonstrated.[20, 21] All studies supported the key role of the *t-m* transformation and associated residual compressive stresses, as well as the balancing act between transformation depth and critical flaw size both affecting strength.[22, 23] As a result, various approaches and techniques have been proposed to assess the depth of the *t-m* transformation after air abrasion, from x-ray diffraction and Raman spectroscopy on cross sections,[22, 24] to sequential polishing and indentation to characterize residual stresses. It was shown that compressive residual stresses are produced to a depth of approximately 10 μm.[25] Meanwhile, the last step in the fabrication of dental restorations usually requires customized staining and glazing, which implies a heat treatment at around 900°C. Even if the duration of this heat treatment is very short (1 min.), studies have shown that when staining and glazing are performed after airborne-particle abrasion, the reverse *m-t* transformation follows,[26] the direct consequence of which is the release of residual compressive stresses. This is associated with a decrease in strength.[17, 19, 27, 28] Varying the sintering temperature, as well as airborne-particle abrasion followed or not by heat treatment therefore represent logical means for changing the crystalline phase assemblage in 3Y-TZP.

Within the field of biomedical applications of brittle ceramics, strength and fracture toughness are recognized properties of paramount importance.[29] The reliability of dental ceramics is classically reported based on Weibull statistics.[30] However, another important concept in the design of bioceramics is that of safety factor, which is defined as the ratio of mean strength to the maximum allowable stress, and is seldom considered in the characterization of dental ceramics.[31, 32] Assuming a Weibull distribution, and choosing a clinically acceptable value for the probability of failure, maximum allowable stresses can be calculated.[31] This information may be helpful in material selection for dental restorations.

The purpose of this in vitro study was to investigate the effect of varying crystalline phase assemblage through sintering temperature and airborne-particle abrasion with or without subsequent heat treatment on reliability, maximum allowable stresses and calculated probability of survival for 3Y-TZP for dental restorations. The null hypothesis was that thermal history alone or in combination with airborne-particle abrasion has no effect on reliability of 3Y-TZP.

MATERIAL AND METHODS

Specimen preparation

Cylindrical 3Y-TZP blanks were produced by cold isostatic pressing of 3Y-TZP powder (TZ-3YE, Tosoh) and pre-sintered at 850°C for 2h. Discs were sectioned from the blanks, randomly assigned to 12 groups of 20 specimens using random number generating software (Microsoft Excel, v. 16.36), sintered at 1350, 1450, 1550 or 1600°C for 2h and furnace-cooled. For each sintering temperature, one group was left as-sintered as control (AS), one group was air-particle abraded (AA) and one group was air-particle abraded and heat treated at 1250°C for 20 minutes (AAHT). This temperature was chosen to ensure that the reverse *m-t* transformation reached full completion. Air-particle abrasion was performed with 50-μm alumina particles, for 1 minute, under a pressure of 2 bars, at a distance of 15 mm and incident angle of 45 degrees.

Crystalline phases – Standard incidence XRD – cubic-related phase

Specimens (n=4 per group) were analyzed by x-ray diffraction (XRD) in Bragg Brentano configuration (SmartLab diffractometer, Rigaku). Patterns were recorded in the 72-76° range (2θ) at a scanning speed of 0.5 deg.min^{-1}, and a step size of 0.04° (λCuKα=1.5406Å). Data were analyzed using Rigaku PDXL-2 software after background subtraction, $K\alpha_2$ elimination and profile fitting. This angular region focuses on *004* and *400* reflections of the *t*-phase, the *400* reflection of the cubic phase and the *004* and *400* reflections of the *t'*, cubic-related phase. The amounts of the various phases were determined from integrated intensities using equation (1).[33]

$$Vc = \frac{It'_{(400)} + It'_{(004)}}{It'_{(400)} + It'_{(004)} + It_{(400)} + It_{(004)}} \quad (1)$$

Where Vc is the volume fraction of the cubic-related phase and I represents the integrated intensity for each listed reflection.

Crystalline phases – GIXRD – transformation depth

Crystalline phases and transformation depth were analyzed by grazing incidence x-ray diffraction (GIXRD) in parallel beam configuration at incidence angles ranging from 1 to 9 omega degrees. GIXRD patterns (n=4 per group) were recorded in the 27-37° (2θ) range, at 0.5 deg.min^{-1}, and a step size of 0.04°. The data were analyzed using Rigaku software as described earlier. The volume fraction of *m*-phase was determined from integrated intensities using equations developed by Garvie and Nicholson,[34] and refined by Toraya.[35] The x-ray penetration depth z was calculated from equation (2) derived from Beer-Lambert's attenuation law:[36]

$$z = \frac{\ln\left(\frac{N}{(S_O + N)}\right)}{-\mu\left(\frac{1}{\sin(\Omega)} + \frac{1}{\sin(2\theta - \Omega)}\right)} \quad (2)$$

Where μ is the x-ray absorption coefficient for 3Y-TZP (0.0640 μm^{-1}),[37] N is the noise level, S_0 the detected signal, Ω the incident angle and $2\theta - \Omega$, the diffracted angle.

Microstructure – grain size

A set of as-sintered discs corresponding to each sintering temperature was polished to a 0.5 μm finish. Specimens were thermally etched prior to examination using an atomic force microscope (AFM, Innova, Bruker) in contact mode. The mean real grain size was determined using the lineal intercept technique[38] using a correction of 1.56, assuming equiaxed grains.[39]

Biaxial flexural strength (BFS)

The mean BFS was measured in air according to ISO standard 6872,[40] using a universal testing machine equipped with a 5kN load cell at a crosshead speed of 0.5 mm/min (Instron 5965) in a piston on ring-of-balls configuration.[41] Piston, fixture and balls were made of 440C stainless steel. The piston diameter was 6.35 mm, the diameter of the supporting balls

was 1.4 mm and the radius of the support circle was 6 mm. The treated side was placed in tension.

Statistical analyses

XRD results were analyzed by ANOVA to detect statistically significant differences between groups. Adjustment for all pairwise group comparisons was made using the Tukey method in conjunction with an overall 0.05 level of significance. BFS results were analyzed using Weibull statistics. The Weibull modulus, characteristic strength, safety factors and maximum allowable stress levels for a probability of survival of 0.999 were calculated for each treatment group,[31] and derived from Weibull analyses. Briefly, a safety factor was first defined as the ratio of the mean strength to the value of the maximum allowable stress. The Weibull distribution was then expressed in terms of mean strength using the following expression (3):

$$P_s = exp\left\{-\left[\left(\frac{\sigma}{\bar{\sigma}}\right)\Gamma\left(1+\frac{1}{m}\right)\right]^m\right\} \quad (3)$$

where P_s is the probability of survival, σ is the strength, $\bar{\sigma}$ is the mean strength, Γ is the gamma function, and m is the Weibull modulus. A given value of $P_s = 0.999$, considered as adequate for dental ceramics, was chosen. The corresponding safety factor (sf) and maximum allowable stress ($\sigma\ allowable$) were calculated using the following expression (4):

$$sf = \frac{\bar{\sigma}}{\sigma\ allowable} = \frac{\Gamma\left(1+\frac{1}{m}\right)}{\left(ln\frac{1}{Ps}\right)^{\frac{1}{m}}} \quad (4)$$

Reversely, after setting a maximum allowable stress of 700 MPa, and knowing the strength and Weibull modulus, the corresponding probability of survival was calculated.

Weibull distributions were compared following an approach derived from Ramadhan *et al.*[42] and Thompson[43]. Likelihood contour plots were obtained using R statistical software.[44] These plots show the 50 to 99% confidence bounds of the estimate for beta (β), the Weibull shape parameter, on the Y-axis, and the 50 to 99% confidence bounds of the estimate of eta (η), the characteristic strength ($\eta=\sigma_0$), on the X-axis. If the 95% contour plots intersect, Weibull parameters are not statistically different at the 95% confidence level.

RESULTS

XRD – cubic and cubic-related *t'*-phase

Representative XRD patterns in standard incidence configuration for as-sintered groups are shown in Figure 1A. A small amount of cubic phase was present in group AS1350. Ka_2 stripping revealed *400* and *004* reflections associated with a cubic-derived *t'*-phase in all other as-sintered groups. Fractions of cubic or cubic-derived *t'*-phase (V_c) are listed in Table 1 and increased linearly with sintering temperature from 10.8 (1.4)% for group AS1350 to 25.2 (1.7)% for group AS1600 (R^2=0.98). There were statistically significant differences in

V_c between all pairs of groups, except between groups AS1550 and AS1600, after adjustment for multiple comparisons.

GIXRD – monoclinic phase as a function of depth

Representative GIXRD patterns are shown in Figure 1B for each treatment group. Airborne-particle abrasion was associated with the formation of *m*-phase for all treated groups, regardless of sintering temperature. This was accompanied by ferroelastic domain switching (FDS), as indicated by the relative intensity reversal for the t_{002} and t_{110} reflections of the *t*-phase. Meanwhile, heat treatment after airborne-particle abrasion led to a reversal of the *t*-*m* transformation, while FDS remained, regardless of sintering temperature. As shown in Figure 2, the relative volume fraction of *m*-phase overall decreased with penetration depth for all AA groups, regardless of sintering temperature. Group AA1350 showed the greatest variability in relative volume fraction (X_m) of *m*-phase as a function of depth, followed by group AA1600. Groups AA1450 exhibited the most consistent relative fractions of *m*-phase as a function of penetration depth. The relative amount of *m*-phase present at the surface of the specimens was largest for group AA1600, followed by AA1550, AA1450 and AA1350.

Microstructure – grain size

Representative atomic force micrographs for each treatment group are displayed in Figure 3. As expected, the mean real grain size increased from 0.35 (0.03) μm (AS1350) to 0.96 (0.12) μm (AS1600). The mean real grain size is indicated on each micrograph. Multiple twinned grains were observed after sintering at 1550°C and above, tentatively identified as *t'* grains (Figure 3E).

Biaxial flexural strength and Weibull analyses

Scatter plots of the BFS data are displayed in Figure 4A. Following adjustment for multiple comparisons, there were no statistically significant differences in mean BFS amongst groups AS1350, AS1450 and AS1600. Airborne-particle abrasion (AA) significantly increased the mean BFS for all groups regardless of sintering temperature. Heat treatment after AA significantly decreased the mean BFS, compared to AA alone. However, the mean BFS of groups AAHT1350 and AAHT1450 was significantly higher than that of matching as-sintered controls.

Weibull moduli (*m*) and calculated characteristic strength values are summarized in Table 1. Weibull plots are displayed in Figure 4B. Reliability, as expressed by *m*, was highest for group AAHT1450 (20.9 (1.3)), followed by AAHT1550 (19.8 (0.9)), and AA1450 (17.6 (0.7)). There were no statistically significant differences found among these 3 groups (unadjusted $P>0.08$). AA alone significantly improved reliability relative to as-sintered condition only for groups AA1450 and AA1600. AA followed by heat treatment significantly increased reliability compared to as sintered groups, except for groups sintered at 1550°C. Groups sintered at 1600°C were all among the lowest 5 in terms of reliability.

Safety factors and maximum allowable stress (*MAS*) for a fixed probability of survival (*Ps*) of 0.999, as well as the calculated *Ps* for a *MAS* of 700 MPa, arbitrarily chosen as an upper value of masticatory stress, are listed in Table 1. Both AA and heat treatment after AA

significantly increased *Wm* for all treatment groups. *Wm* was highest for group AAHT1450, followed by AAHT1550, AA1450, AAHT1350 and AA1550.

The calculated *MAS* corresponding to a *Ps* of 0.999 was 1047 MPa for group AA1450, followed by 916 MPa for group AA1550, 887 MPa for group AAHT1450, and 799 MPa for group AAHT1550. The group associated with the lowest *MAS* was AS1600, with 404 MPa, followed by AS1350, with a *MAS* of 452 MPa. The calculations of the *Ps* for a set *MAS* of 700 MPa followed the same trend, with the lowest *Ps* for group AS1600 (P=0.9542) followed by AS1350 (P=0.9658). All other groups had a *Ps* greater than 0.98 for this *MAS* condition.

Likelihood contour plots of beta (β), the Weibull shape parameter, as a function of eta ($\eta=\sigma_0$), the characteristic strength, are shown in Figure 5. Contour plots intersected for groups AS1350, AS1450, AS1600 and AAHT1600 in a first cluster, and groups AAHT1350, AAHT1450 and AS1550 in a second cluster, indicating no significant difference in Weibull parameters within these two clusters, while all other groups were significantly different (P<0.05).

DISCUSSION

The purpose of this study was to investigate the effect of phase assemblage on reliability of 3Y-TZP. Our results demonstrate that phase assemblage modulated either by sintering temperature or post-processing treatment affects the reliability of 3Y-TZP ceramics. Therefore, the null hypothesis stating that phase assemblage had no effect on reliability was rejected.

Grain size and fraction of cubic-derived phase

The variation observed in grain size as a function of sintering temperature is in line with previously published data for 3Y-TZP. Standard incidence XRD in the 72-76° range revealed the presence of cubic-derived *t'*-phase in as-sintered groups, the volume fraction of which increased linearly with sintering temperature from 1450 to 1600°C. These results are in agreement with the literature.[10, 33, 42] Scott[42] first outlined the eventuality of a diffusion-less shear transformation from cubic to tetragonal in Y-TZP, leading to the formation of a second tetragonal phase, *t''*. This was further confirmed by electron diffraction.[43] XRD studies later demonstrated that when TZP ceramics are sintered at temperatures in excess of 1450°C, some or all of the cubic zirconia transforms into *t'*-phase after cooling.[33, 44] This non-transformable *t'* phase is characterized by a lower tetragonality and a higher yttrium content than the transformable *t*-phase.[45]

Relative fraction of monoclinic phase vs. depth

GIXRD experiments revealed that the relative volume fraction of *m*-phase as a function of depth was most variable for group AA1350, followed by AA1600, AA1550 and AA1450. This variability explains the results obtained for the Weibull modulus, for which the same ranking applied. The reliability of 3Y-TZP therefore appears to correlate with how reliably the *t*-*m* transformation occurred, rather than be linked to the relative fraction of *m*-phase formed. Furthermore, these results indicate that sintering temperature and therefore grain

size, appears to influence the variability of the transformation. This is consistent with the observation that larger grains are more prone to transformation and transform more reliably.[13]

Biaxial flexural strength – Weibull modulus

Results obtained for the mean BFS after airborne-particle abrasion, or after airborne-particle abrasion followed by heat treatment can be readily explained by the presence of compressive residual stresses after the *t-m* transformation triggered by air-particle abrasion and subsequent elimination of these stresses following heat treatment. This general trend was observed, regardless of sintering temperature. However, numerous studies have shown that the *t-m* transformation is not the only strengthening mechanism in 3Y-TZP and that ferro-elastic domain switching (FDS) is also responsible for a significant amount of strengthening. FDS corresponds to a reorientation of ferroelastic domains and is evidenced by a reversal of the intensity of the *(200)* and *(002)* x-ray reflections for 3Y-TZP. Importantly, as opposed to the *t-m* transformation, FDS is not reversible. Based on our experimental design, as-sintered groups only undergo localized *t-m* transformation upon fracture. Meanwhile AA specimens have already undergone some degree of *t-m* transformation and irreversible FDS, fracture occurrence therefore requires that both strengthening mechanisms be overcome. In air-particle abraded and heat-treated specimens, the reverse *m-t* transformation has occurred but FDS is no longer available as a strengthening mechanism, leaving the *t-m* transformation as the only mechanism left for strengthening. By comparing strength values, the contribution of each strengthening mechanism can be estimated. BFS results show that FDS contribution was highest for AA1350 (39.4%), followed by AA1450 (30.4%), AA1600 (23.4%) and AA1550 (11.6%). Concurrently the *t-m* transformation contribution decreased from AA1350 (15.6%) followed by AA1450 (14.6%), AA1550 (9.7%), and AA1600 (0.5%). These results are in line with the measured fraction of non-transformable *t'*-phase, which was found to be highest in groups sintered at 1600°C.

As mentioned earlier, the values obtained for the Weibull modulus of the AA groups match the variability in the fraction of *m*-phase measured as a function of depth, with group AA1350 having the lowest Weibull modulus of all AA groups and the highest variability in *m*-phase fraction as a function of depth. This was indirectly confirmed by the fact that the Weibull modulus of the corresponding air abraded and heat-treated group (AAHT1350) was significantly higher. This is in line with studies by Chintapalli *et al.*,[22, 25] demonstrating the presence of a non-homogeneous transformation gradient after air-particle abrasion of 3Y-TZP. Higher Weibull moduli were also observed for groups AAHT1450 and AAHT1550, compared to AA1450 and AA1550. This trend could be due to the reverse *m-t* transformation and the elimination of the associated compressive stresses. Meanwhile, it has been shown that heat treatment after AA or surface grinding leads to surface recrystallization into smaller grains (20-200 nm).[38,39] These nano-sized grains reduce the susceptibility of zirconia to low temperature degradation and may also be associated with a more even surface flaw distribution thereby explaining the observed increase in Weibull modulus.[16]

Maximum allowable stress – probability of survival

Maximum allowable stresses (MAS) and survival probability (*Ps*) calculations clearly indicate that groups AS1350 and AS1600 were associated with the lowest MAS for *Ps*=0.999 and the lowest *Ps* for MAS=700 MPa. Meanwhile groups exhibiting the highest MAS were AA1450, AAHT1450, AA1550 and AAHT1550. These same groups had a *Ps* of 1 when MAS was fixed at 700 MPa. Although core fractures are infrequent with 3Y-TZP dental restorations,[40] the present study demonstrated that sintering temperatures of 1350 and 1600°C are not optimal for zirconia ceramics stabilized with 3 mol.% yttria.

CONCLUSIONS

Within the limitations of this in vitro study the following conclusions may be drawn:

- The sintering temperature affected the phase assemblage in as-sintered 3Y-TZP, with a linear increase in the amount of cubic or cubic-derived non-transformable *t'*-phase in the 1350-1600°C range. The pattern of biaxial flexural strength results indicated that ferro-elastic domain switching was a dominant strengthening mechanism in 3Y-TZP after airborne-particle abrasion.
- FDS strengthening contribution was largest for group AA1350 and decreased with increasing sintering temperature. The increase in the fraction of non-transformable *t'*-phase with sintering temperature was paired with a decrease in flexural strength for all groups sintered at 1600°C.

REFERENCES

1. Zhang Y, Lawn BR. Novel Zirconia Materials in Dentistry. J Dent Res 2018;97:140–7. [PubMed: 29035694]
2. Zhang Y Making yttria-stabilized tetragonal zirconia translucent. Dent Mater 2014;30:1195–203. [PubMed: 25193781]
3. Sailer I, Balmer M, Husler J, Hammerle CHF, Kanel S, Thoma DS. 10-year randomized trial (RCT) of zirconia-ceramic and metal-ceramic fixed dental prostheses. J Dent 2018;76:32–9. [PubMed: 29807060]
4. Bomicke W, Rammelsberg P, Zenthofer A, Ohlmann B. Clinical performance of zirconia-ceramic cantilever fixed partial dentures-Longitudinal nine-year results from a prospective, randomized, controlled pilot study. J Prosthodont Res 2019;63:334–9. [PubMed: 30803899]
5. Denry I, Kelly JR. State of the art of zirconia for dental applications. Dent Mater 2008;24:299–307. [PubMed: 17659331]
6. Chevalier J What future for zirconia as a biomaterial? Biomaterials 2006;27:535–43. [PubMed: 16143387]
7. Chevalier J, Grémillard L, Virkar AV, Clarke DR. The Tetragonal-Monoclinic Transformation in Zirconia: Lessons Learned and Future Trends. J Am Ceram Soc 2009;92:1901–20.
8. Beuer F, Edelhoff D, Gernet W, Sorensen JA. Three-year clinical prospective evaluation of zirconia-based posterior fixed dental prostheses (FDPs). Clin Oral Investig 2009;13:445–51.
9. Sailer I, Feher A, Filser F, Luthy H, Gauckler LJ, Scharer P et al. Prospective clinical study of zirconia posterior fixed partial dentures: 3-year follow-up. Quintessence Int 2006;37:685–93. [PubMed: 17017630]
10. Matsui K, Horikoshi H, Ohmichi N, Ohgai M, Yoshida H, Ikuhara Y. Cubic-Formation and Grain-Growth Mechanisms in Tetragonal Zirconia Polycrystal. J Am Ceram Soc 2003;86:1401–8.
11. Ruiz L, Readey MJ. Effect of heat-treatment on grain size, phase assemblage, and mechanical properties of 3 mol% Y-TZP. J Am Ceram Soc 1996;79:2331–40.

12. Eichler J, Rodel J, Eisele U, Hoffman M. Effect of Grain Size on Mechanical Properties of Submicrometer 3Y-TZP: Fracture Strength and Hydrothermal Degradation. J Am Ceram Soc 2007;90:2830–6.
13. Suresh A, Mayo MJ, Porter WD, Rawn CJ. Crystallite and grain-size-dependent phase transformations in yttria-doped zirconia. J Am Ceram Soc 2003;86:360–2.
14. Stawarczyk B, Ozcan M, Hallmann L, Ender A, Mehl A, Hammerlet CHF. The effect of zirconia sintering temperature on flexural strength, grain size, and contrast ratio. Clin Oral Investig 2013;17:269–74.
15. Kato H, Matsumura H, Atsuta M. Effect of etching and sandblasting on bond strength to sintered porcelain of unfilled resin. J Oral Rehabil 2000;27:103–10. [PubMed: 10672145]
16. Borges GA, Sophr AM, de Goes MF, Sobrinho LC, Chan DCN. Effect of etching and airborne particle abrasion on the microstructure of different dental ceramics. J Prosthet Dent 2003;89:479–88. [PubMed: 12806326]
17. Kosmac T, Oblak C, Jevnikar P, Funduk N, Marion L. Strength and reliability of surface treated Y-TZP dental ceramics. J Biomed Mater Res 2000;53:304–13. [PubMed: 10898871]
18. Kosmac T, Oblak C, Jevnikar P, Funduk N, Marion L. The effect of surface grinding and sandblasting on flexural strength and reliability of Y-TZP zirconia ceramic. Dent Mater 1999;15:426–33. [PubMed: 10863444]
19. Kosmac T, Oblak C, Marion L. The effects of dental grinding and sandblasting on ageing and fatigue behavior of dental zirconia (Y-TZP) ceramics. J Eur Ceram Soc 2008;28:1085–90.
20. Cotic J, Jevnikar P, Kocjan A, Kosmac T. Complexity of the relationships between the sintering-temperature-dependent grain size, airborne-particle abrasion, ageing and strength of 3Y-TZP ceramics. Dent Mater 2016;32:510–8. [PubMed: 26792621]
21. Caravaca CF, Flamant Q, Anglada M, Gremillard L, Chevalier J. Impact of sandblasting on the mechanical properties and aging resistance of alumina and zirconia based ceramics. J Eur Ceram Soc 2018;38:915–25.
22. Chintapalli RK, Marro FG, Jimenez-Pique E, Anglada M. Phase transformation and subsurface damage in 3Y-TZP after sandblasting. Dent Mater 2013;29:566–72. [PubMed: 23537568]
23. Wongkamhaeng K, Dawson DV, Holloway JA, Denry I. Effect of Surface Modification on In-Depth Transformations and Flexural Strength of Zirconia Ceramics. J Prosthodont 2019;28:E364–E75. [PubMed: 29741238]
24. Sato H, Yamada K, Pezzotti G, Nawa M, Ban S. Mechanical properties of dental zirconia ceramics changed with sandblasting and heat treatment. Dent Mater J 2008;27:408–14. [PubMed: 18717169]
25. Chintapalli RK, Rodriguez AM, Marro FG, Anglada M. Effect of sandblasting and residual stress on strength of zirconia for restorative dentistry applications. J Mech Behav Biomed 2014;29:126–37.
26. Guazzato M, Quach L, Albakry M, Swain MV. Influence of surface and heat treatments on the flexural strength of Y-TZP dental ceramic. J Dent 2005;33:9–18. [PubMed: 15652163]
27. Denry IL, Holloway JA. Microstructural and crystallographic surface changes after grinding zirconia-based dental ceramics. J Biomed Mater Res B-Appl Biomater 2006;76B:440–8.
28. Passos SP, Linke B, Major PW, Nychka JA. The effect of air-abrasion and heat treatment on the fracture behavior of Y-TZP. Dent Mater 2015;31:1011–21. [PubMed: 26117560]
29. Kelly JR. Future of dental biomaterials: Gazing into Bob's crystal ball J Prosthet Dent Accepted.
30. Quinn JB, Quinn GD. A practical and systematic review of Weibull statistics for reporting strengths of dental materials. Dent Mater 2010;26:135–47. [PubMed: 19945745]
31. Wachtman JB. Mechanical properties of ceramics. 1st ed. New York: John Wiley & Sons, Inc.; 1996.
32. Zhang ZP, Chen JN, Li E, Li W, Swain M, Li Q. Topological design of all-ceramic dental bridges for enhancing fracture resistance. Int J Numer Meth Bio 2016;32.
33. Paterson A, Stevens R. Phase analysis of sintered yttria-zirconia ceramics by x-ray diffraction. J Mater Res 1986;1:295–9.
34. Garvie RC, Nicholson PS. Phase analysis in zirconia systems. J Am Ceram Soc 1972;55:303–5.

35. Toraya H, Yoshimura M, Somiya S. Quantitative analysis of monoclinic-stabilized cubic ZrO_2 systems by X-ray diffraction. J Am Ceram Soc 1984;67:C183–C4.

36. Liu JD, Saw RE, Kiang YH. Calculation of Effective Penetration Depth in X-Ray Diffraction for Pharmaceutical Solids. J Pharm Sci 2010;99:3807–14. [PubMed: 20665844]

37. Hubbell J, Sheltzer S. X-Ray Mass Attenuation Coefficients - NIST Standard Reference Database 126. NIST; 2019.

38. International Standards Organization. Implants for surgery - Ceramic materials based on yttria-stabilized tetragonal zirconia (Y-TZP). ISO 13356:2015. Geneva, Switzerland: ISO/TC 150/SC 1 Materials; 2015.

39. Mendelson M Average grain size in polycrystalline ceramics. J Am Ceram Soc 1969;52:443–6.

40. International Standards Organization. ISO6872:2015 - Dentistry - Ceramic Materials. Geneva, Switzerland: ISO/TC 106/SC 2 Prosthodontic materials; 2015. p. 6–15.

41. Denry IL, Peacock JJ, Holloway JA. Effect of heat treatment after accelerated aging on phase transformation in 3Y-TZP. Journal of Biomedical Materials Research Part B-Applied Biomaterials 2010;93B:236–43.

42. Scott HG. Phase relationships in the zirconia-yttria system. J Mater Sci 1975;10:1527–35.

43. Andersson CA, Greggi J, Gupta TK. Diffusionless transformations in zirconia alloys, in “Science and technology of zirconia II”. United States: American Ceramic Society, Inc; 1984.

44. Leach CA. Development of the secondary tetragonal phase in conventionally sintered yttria-TZP ceramics. J Mater Sci Lett 1987:303–4.

45. Sheu TS, Tien TY, Chen IW. Cubic-to-tetragonal (t’) transformation in zirconia-containing syztems J Am Ceram Soc 1992;75:1108–16.

CLINICAL IMPLICATIONS

When selecting a sintering program for zirconia ceramics stabilized with 3 mol. % yttria, technicians and clinicians should keep in mind that sintering at a temperature of 1600°C is detrimental to both strength and reliability of 3Y-TZP and should therefore be avoided. Meanwhile, airborne-particle abrasion is confirmed as a recommended processing step as it was found to be associated with an increase in both strength and reliability, particularly when 3Y-TZP was sintered at 1350°C. These results were explained by the crystalline phase assemblage.

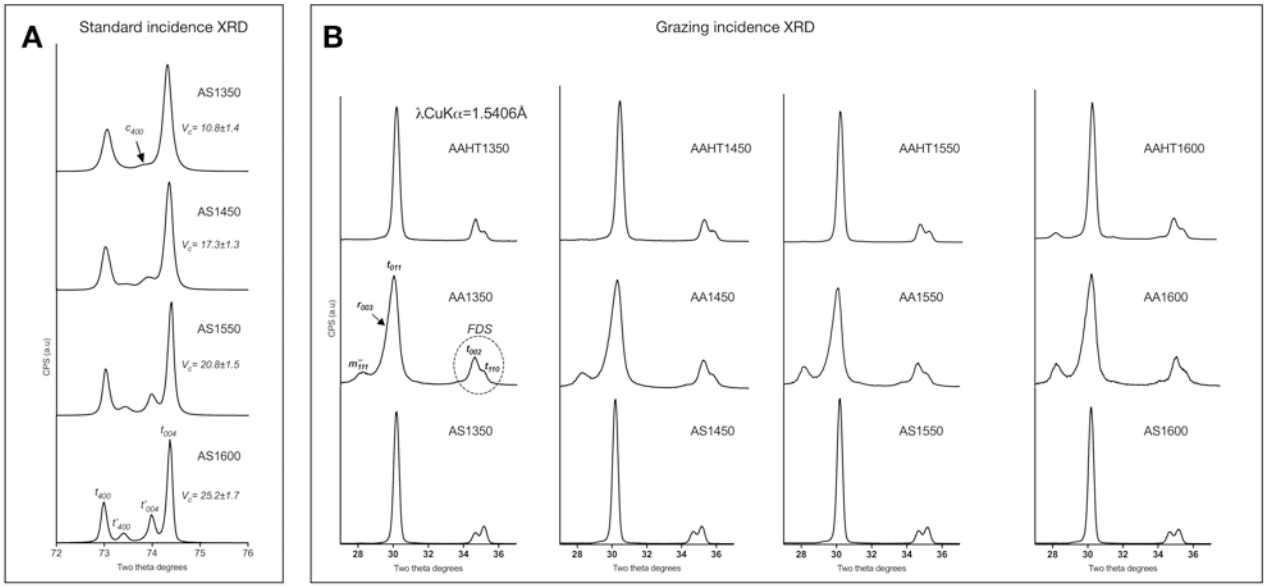

Figure 1.

A: Standard incidence X-ray diffraction patterns of the various as-sintered groups in the 72-76° (2θ) range; B: Grazing incidence x-ray diffraction patterns of the various experimental groups in the 27-37° (2θ) range.

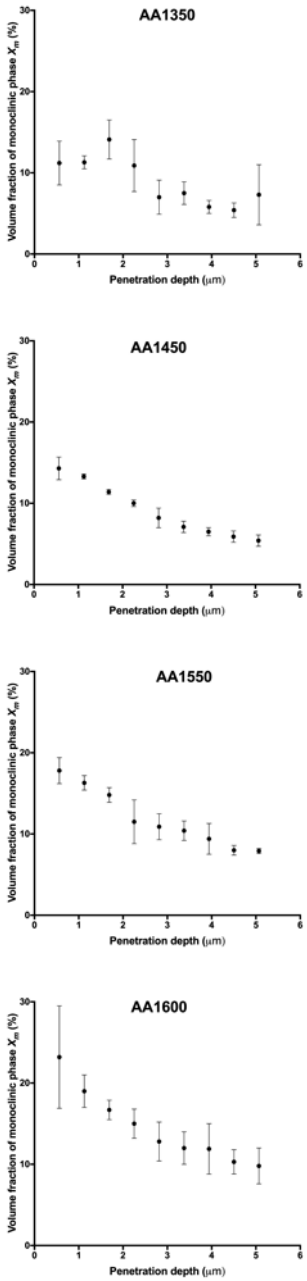

Figure 2.

As-measured volume fractions of monoclinic (X_m) phase as a function of depth for air-particle abraded groups.

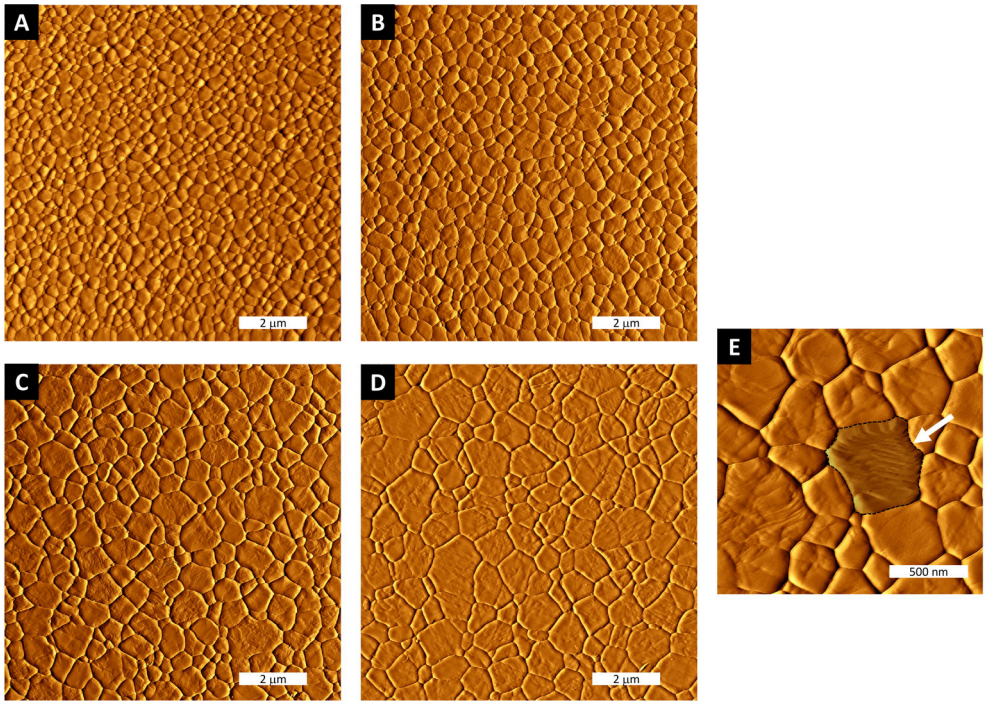

Figure 3.

Representative atomic force micrographs for the various groups (contact mode). A: Sintered at 1350°C; B: Sintered at 1450°C; C: Sintered at 1550°C; D: Sintered at 1600°C. E: Higher magnification of specimen sintered at 1550°C, arrow indicates a twinned grain tentatively identified as *t'*-phase.

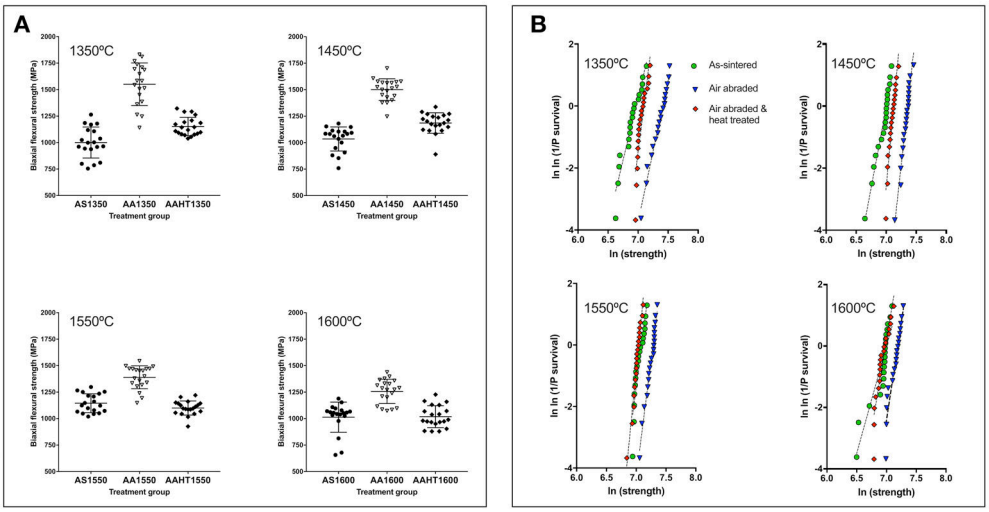

Figure 4.

A: Scatter plots of the biaxial flexural strength values for each treatment group (horizontal bars represent mean ± SD); B: Weibull plots of the various treatment groups.

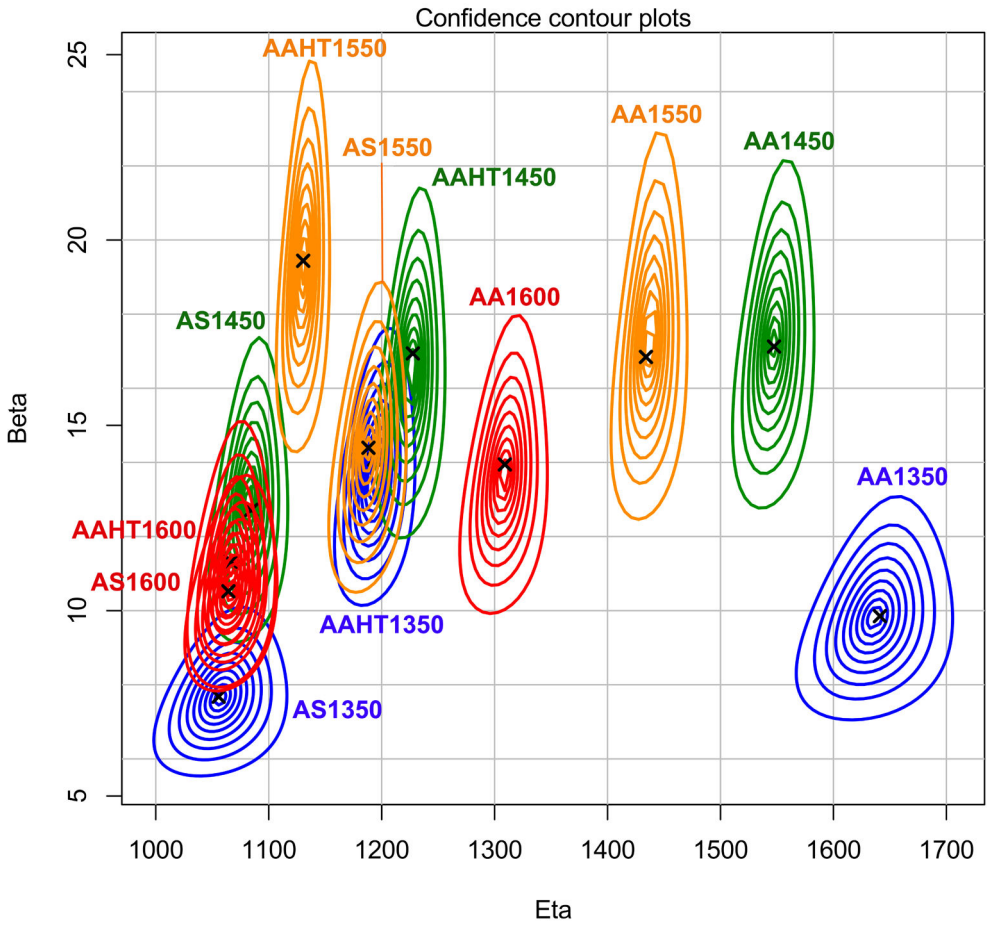

Figure 5.

Confidence contour plots at the 0.5, 0.6, 0.7, 0.8, 0.9, 0.95, 0.975 and 0.99 confidence levels for each experimental group. Intersecting contour plots indicate no significant difference in Weibull parameters.

Table 1.

Volume fraction *(Xc-t')* of cubic-derived *c* and *t'*-phase, mean biaxial flexural strength (BFS), characteristic strength (σ_0) and Weibull modulus *(m)* for the various treatment groups. Calculated maximum allowable stress (MAS) for a fixed probability of survival P_s of 0.999, safety factor and P_s associated with a fixed MAS of 700 MPa for each treatment group.

Group	*Xc-t'* (SD) (%)	BFS (SD) (MPa)	σ_0 (SD) (MPa)	Weibull modulus *m* (SD)	MAS (MPa)	Safety factor	P_s
					P_s=0.999	(MAS=700 MPa)	
AS1350	10.8 (1.4)[a]	1000 (146)[a]	1061 (6)	8.1 (0.5)[a]	452	1.429	0.9658
AA1350		1553 (201)[e]	1656 (5)	9.1 (0.3)[g]	767	2.219	0.9996
AAHT1350		1156 (87)[bc]	1210 (7)	15.4 (1.7)[c]	762	1.651	0.9997
AS1450	17.3 (1.3)[b]	1036 (114)[a]	1101 (4)	13.3 (0.5)[a]	552	1.480	0.9885
AA1450		1502 (102)[de]	1566 (3)	17.6 (0.7)[f]	1047	2.146	1.0000
AAHT1450		1202 (69)[bc]	1249 (3)	20.9 (1.3)[c]	887	1.717	1.0000
AS1550	20.8 (1.5)[c]	1147 (89)[bc]	1204 (7)	15.0 (1.4)[c]	751	1.639	0.9996
AA1550		1391 (108)[d]	1458 (3)	15.2 (0.6)[e]	916	1.987	1.0000
AAHT1550		1102 (66)[ab]	1147 (2)	19.8 (0.9)[b]	799	1.574	0.9999
AS1600	25.2 (1.7)[c]	1015 (143)[a]	1099 (14)	7.0 (0.8)[a]	404	1.450	0.9542
AA1600		1258 (115)[c]	1327 (6)	12.8 (0.9)[d]	764	1.797	0.9997
AAHT1600		1020 (103)[a]	1074 (6)	11.6 (1.0)[a]	589	1.457	0.9925

Identical letters denote no statistically significant difference after adjustment for multiple comparisons